Modelling of dual-frequency capacitive discharges

M. M. Turner [a,*], P. Chabert [b]

[a] *National Centre for Plasma Science and Technology and School of Physical Sciences, Dublin City University, Ireland*
[b] *LPTP, Ecole Polytechnique, France*

Abstract

We discuss electron heating mechanisms in the sheath regions of dual-frequency capacitive discharges, with the aims of identifying the dominant mechanisms and supplying closed-form expressions from which the heating power can be estimated. We show that the heating effect produced by either Ohmic or collisionless heating is much larger when the discharge is excited by a superposition of currents at two frequencies than if either current had acted alone. This coupling effect occurs because the lower frequency current, while not directly heating the electrons to any great extent, strongly affects the spatial structure of the discharge in the sheath regions. From these results it follows that the ion flux cannot generally be independent of the low-frequency current density, and hence that separate control of the ion energy and flux must be a more complicated procedure than is sometimes suggested.

Key words: radio-frequency, capacitive, dual-frequency, particle-in-cell simulation

1. Introduction

Great interest is presently directed towards capacitive discharges excited by a superposition of currents at two or more frequencies. This interest is motivated by a desire to control the plasma parameters with more freedom than is possible when only a single frequency is employed. In a typical dual-frequency discharge, the two frequencies are disparate, with a ratio of at least ten. Moreover, the current density at the higher frequency is larger than that at the lower frequency. As the impedance is predominantly capacitive, and therefore decreasing with frequency, one typically finds that the voltage associated with the lower frequency is larger than the voltage associated with the higher frequency. The advantage of this configuration is that the plasma density, and hence the ion flux at the plasma boundary, depends primarily on the current density, and this is controlled by the higher frequency, while the ion energy at the boundary depends mainly on the voltage, and this is controlled by the lower frequency. Hence one can hope to exert separate control over the ion flux and energy by appropriately manipulating the higher and lower frequency current densities. Since the ion flux and energy are crucial parameters in many applications, this is an important advantage. Of course, in practice one does not achieve independent control of these two parameters. Various physical mechanisms produce coupling between the two frequencies, and these effects have been explored in general terms in a number of recent papers, *e.g.* [1–6]. The purpose of the present paper is to discuss the electron heating mechanisms that operate in dual-frequency discharges—in particular, to elucidate their nature and significance, and as far as possible supply convenient formulae that may be used as elements in a comprehensive theoretical understanding of these discharges.

In the discussion that follows, we focus on the

* Corresponding author.
Email address: miles.turner@dcu.ie (M. M. Turner).

sheath region, where we assume that the spatial and temporal structure is adequately described by the analytical model of [7,8]. We adopt from these models a simplified representation of the spatial structure of the sheath, in which the transition between the quasi-neutral plasma and the space-charge sheath is modelled as a step-function in the electron density. Since the ion density is assumed to be time independent, the sheath dynamics are captured by specifying the position of this electron density step as a function of time. In the discussions that follow, we denote the position of this electron sheath edge by $x = s(t)$, and we adopt the convention that the ion sheath edge, where the ions reach the Bohm velocity, is at $x = 0$, so that the electrode is at $x = s_{\max}$. In a dual-frequency discharge, the trajectory of the electron sheath edge is complex, but bounded in the range $0 \leq s(t) \leq s_{\max}$. We assume that the current passing through the sheath is the superposition of two frequencies, so that

$$J(t) = -\tilde{J}_l \sin \omega_l t - \tilde{J}_h \sin \omega_h, \tag{1}$$

where $\tilde{J}_{l,h}$ and $\omega_{l,h}$ are the current densities and angular frequencies of the two components. (The surprising sign convention is chosen for consistency with previous works [9,7].) Robiche *et al* [7] have shown that under these assumptions, the sheath dynamics are adequately described by three dimensionless parameters, the ratio of current frequencies, $\alpha \equiv \omega_h/\omega_l$, the ratio of current densities, $\beta \equiv \tilde{J}_h/\tilde{J}_l$, and $H_l \equiv \tilde{J}_l^2/\pi T \omega_l^2 n_0$, subject to approximations that hold when $\beta/\alpha \ll 1$. The parameter H was introduced in the single frequency sheath model of Lieberman [9]. An important point is that the equivalent of the Lieberman H parameter for this dual-frequency sheath model does not depend on the higher frequency parameters, ω_h and $\tilde{J}_h$, which shows that the lower-frequency essentially controls the spatial structure of the sheath. As we will see, this is a crucial point with profound implications for the interaction of the frequencies in a dual-frequency discharge.

2. Collisionless heating

We consider a plasma consisting of electrons and one species of positive ion. Both electrons and ions are assumed collisionless. An electrode is in contact with the plasma, and this electrode carries a net current density given by eq. 1. We assume that the collisionless heating effect occurs in the electron fluid,

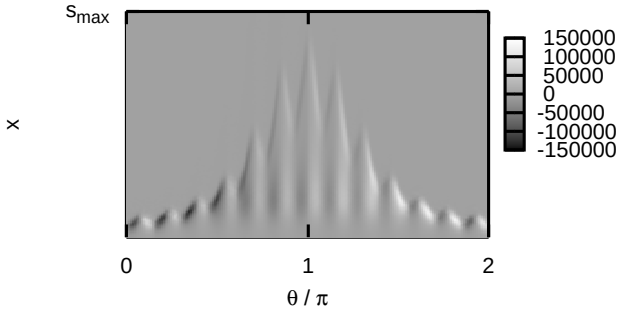

Fig. 1. Collisionless heating power as a function of space and time, calculated by the particle simulation, with $\tilde{J}_l = 10$ A m^{-2}, $\omega_l = 2\pi \times 2$ MHz, $\tilde{J}_h = 20$ A m^{-2} and $\omega_l = 2\pi \times 26$ MHz, and the plasma parameters discussed in the text. The ion sheath edge is at $x = 0$ and the electrode is at $x = s_{\max}$.

in the region between the electron and ion sheath edges, as in [10]. By extending the theory of that paper [11], we can show that the effective temperature of electrons in the sheath can be expressed as a power series in the form:

$$\tau = \tau^{(0)} + \delta_l \tau_l^{(1)} + \delta_h \tau_h^{(1)} + \delta_l^2 \tau_l^{(2)} + \delta_h^2 \tau_h^{(2)} + \delta_l \delta_h \tau_{hl}^{(2)} + \mathrm{O}(\delta_{l,h}^3), \tag{2}$$

where $\tilde{u}_l = \tilde{J}_l/en_0$, $\tau = T/T_b$, and the functions $\tau^{(n)}$ are given by:

$$\tau^{(0)} = 1 \tag{3}$$

$$\tau_l^{(1)} = 2 \ln \eta \sin \theta \tag{4}$$

$$\tau_h^{(1)} = 2 \ln \eta \sin \alpha\theta \tag{5}$$

$$\tau_l^{(2)} = -(1 - \cos\theta) \frac{d\tau_l^{(1)}}{d\theta} \tag{6}$$

$$\tau_h^{(2)} = -\frac{1}{\alpha}(1 - \cos\alpha\theta) \frac{d\tau_h^{(1)}}{d\theta} \tag{7}$$

$$\tau_{lh}^{(2)} = -(1 - \cos\theta) \frac{d\tau_h^{(1)}}{d\theta} - \frac{1}{\alpha}(1 - \cos\alpha\theta) \frac{d\tau_l^{(1)}}{d\theta}. \tag{8}$$

We can now express the sheath heating power per unit area as:

$$\langle S_{lh} \rangle = -\langle Q_0 \rangle = 2Q_b \tau(\tau - 1) \tag{9}$$

$$= 2Q_b \left\langle \delta_l^2 \left(\tau_l^{(2)} + {\tau_l^{(1)}}^2 \right) + \delta_h^2 \left(\tau_h^{(2)} + {\tau_h^{(1)}}^2 \right) \right\rangle, \tag{10}$$

where $Q_b = \frac{1}{4} n_0 \bar{v}_b T_b$, $\bar{v}_b = \sqrt{8T/\pi m_e}$, the subscript s denotes quantities defined at the electron

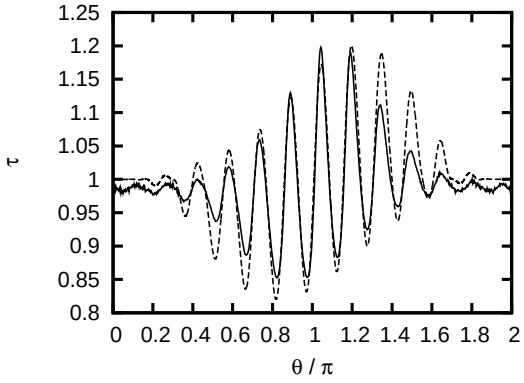

Fig. 2. Temperature of electrons in the sheath computed from the analytic theory of the text (solid line) and from the particle-in-cell simulation (dashed line), for the conditions noted in fig. 1.

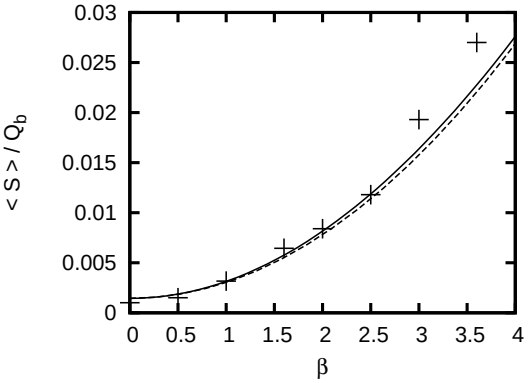

Fig. 3. Normalized collisionless heating power as a function of $\beta \equiv \tilde{J}_h/\tilde{J}_l$, with $\tilde{J}_h$ as the parameter varied (so that H_l is constant) and with $\alpha = \omega_h/\omega_l = 13$.

sheath edge and T_b is the temperature of the electron flux incident from the bulk plasma. We note that $\langle \tau_l^{(1)} \rangle = \langle \tau_h^{(1)} \rangle = \langle \tau_{lh}^{(2)} \rangle = 0$. The instantaneous heating power in eq. 9 is not identical with the integral of the product JE from $x = 0$ to $x = s(t)$, because both the drift energy and the thermal energy of the electron fluid in this region vary with time. However, the time average of this spatial integral of JE and the time average given by eq. 9 are identical.

An approximate but compact compact expression for the net heating when both frequencies act together can be shown to be:

$$\langle S_{lh} \rangle \approx 2Q_b \left(\delta_l^2 + 1.1\delta_h^2\right) \frac{36H_l}{55 + H_l}. \tag{11}$$

It is remarkable that this expression is structurally identical to the result obtained by quite different arguments in [12].

We will now discuss the predictions of this model with reference to particle-in-cell simulations [13]. The physical parameters used in these calculations are $n_0 = 5 \times 10^{15}$ m^{-3} and $T_b = 30000$ K. Except where otherwise implied, $\omega_l = 2\pi \times 2$ MHz, $\omega_h = 2\pi \times 26$ MHz, $\tilde{J}_l = 10$ A m^{-2} and $\tilde{J}_h = 36$ A m^{-2}

Indications of the general character of the heating effect, and the consistency of the simulations with the model, are shown in figs. 1 and 2. Fig 1 is an example of the heating power per unit area computed from the simulation. This figure shows that the heating power reaches a positive maximum during the expanding phase of the low-frequency sheath, where $\pi < \theta < 2\pi$, a feature which is also seen in the analytical model. In fig. 2, we compare the sheath electron temperature from the simulation with the analytical model, and we find generally good agreement. Fig. 3 shows excellent agreement between the simulations and the model for a moderate value of α.

Our model entails surprising predictions: Namely, that the heating power does not depend on the parameter H_h and cannot be expressed as if the two frequencies acted additively. As we suggested above, the spatial structure of the sheath is controlled by low-frequency parameters, with the result that the heating power is enhanced when the two frequencies act together, because $F_2(H_l) \gg F_2(H_h)$ and $\delta_h^2 \gg \delta_l^2$, where we recall that $\delta_{l,h} \propto \tilde{J}_{l,h}$. Specifically, since

$$\frac{\langle S_{lh} \rangle}{\langle S_l \rangle + \langle S_h \rangle} \approx \frac{1 + 1.1\beta^2}{1 + \beta^4/\alpha^2} \tag{12}$$

when $H_{l,h}$ are not too large so $A_2(H) \sim 36H/55$, the maximum enhancement is approximately $(1+\alpha)/2$, which occurs when $\beta \approx \sqrt{\alpha}$. These parameters are within the typical range of current experiments. The enhancement occurs because the application of the low frequency changes the sheath structure, allowing the high frequency to explore a much wider dynamic range of plasma density. In fig. 4, we compare the heating effect produced by each frequency separately with their combined effect, showing that the predicted enhancement does exist. In the case shown, which is close to the predicted maximum with $\beta/\sqrt{\alpha} \sim 1$, the enhancement factor is approximately 5, compared to the predicted 7. The discrepancy is mostly because H_h is significantly less than 1, and the single frequency theory is not highly accurate in that case. We note that the application of the low frequency produces an appreciable expansion of the volume of plasma affected by the heating process.

The theory we have been discussing cannot presently be extended by formal means to the interesting limit $J_l \to 0$, because the sheath model of [7] is not valid in that case. However, a simple ansätz allows us to construct an extension that connects the present dual frequency theory smoothly to the single frequency theory of [10]. This ansätz entails the definition of an effective value of the parameter H that is given by

$$H_{\text{eff}} = \sqrt{H_l^2 + H_h^2}. \tag{13}$$

If this effective value is inserted into eq. 11, an expression is obtained that is essentially identical with the present theory when $H_l \gg H_h$, almost identical with the results of [10] when $H_l \ll H_h$, and reasonably behaved in the transition between these two regimes. In fig. 5, we compare this generalized expression with simulation results.

3. Ohmic heating

We now turn to the calculation of the Ohmic heating component. In general, the instantaneous Ohmic heating power per unit volume dissipated in a plasma with density n and electron collision frequency ν_e is

$$P_{\text{ohmic}} = \frac{m_e \nu_e J^2(t)}{n e^2} \tag{14}$$

where J is the current density, and we have assumed that any ionic contribution to the heating effect is negligible. The Ohmic power dissipation per unit area within the sheath is now found by integrating from the ion sheath edge to the electron sheath edge at $s(t)$:

$$S_{\text{ohmic}}(t) = \frac{m_e \nu_e J^2(t)}{e^2} \int_0^{s(t)} \frac{dx}{n(x)} \tag{15}$$

$$= J^2(t) \frac{m_e \nu_e}{e^2} \int_0^{\phi(t)} \frac{d\phi'}{n(\phi')} \frac{dx}{d\phi'} \tag{16}$$

where $\phi = \omega_l t$ is the independent variable of the Lieberman [9] and Robiche [7] sheath models. These expressions hold for any sheath model. If we assume that the sheath structure is adequately described by the analytical dual frequency sheath model of [7], then we have closed, albeit complex, expressions for $dx/d\phi$ and $n(\phi)$. The problem of calculating the time-averaged Ohmic heating thus becomes a double quadrature that can be written:

$$\bar{S}_{\text{ohmic}} = \frac{32}{\pi} Q_b \delta_l^3 \left(\frac{\nu_e}{\omega_l}\right) F_2(\alpha, \beta, H_l). \tag{17}$$

The integrations entailed in the function F_2 can be carried out formally, but the resulting expressions are not useful [7]. A compact and convenient approximation can however be obtained by considering the limit $\alpha \gg 1$, in which case the high frequency terms can be substituted by constants. The remaining integrations can then be carried out without further approximation to find:

$$F_2 \approx A_2 = \left[\frac{1}{2}\left(1+\beta^2\right) + \frac{1}{\pi}\left(\frac{512}{675} + \frac{32}{27}\beta^2\right) H_l + \left(\frac{14912}{165375} + \frac{1336}{3375}\beta^2\right) H_l^2\right] .. \tag{18}$$

The result eq. 18 shows that Ohmic heating, like collisionless heating, is enhanced by the combination of two frequencies. The physical mechanism of the enhancement is similar—when the lower frequency is applied, the spatial structure of the sheath region is modified, and in particular the ion density near the boundary is greatly reduced. When the sheath is collapsed, and these regions are populated by electrons, the higher frequency current is conducted through a much more tenuous plasma than would be the case if the lower frequency was absent. The Ohmic heating effect is thereby dramatically enhanced.

4. Ohmic and collisionless heating

We have seen that both collisionless and Ohmic heating are enhanced when currents at two disparate frequencies are superimposed, and that the mechanism of this enhancement is the control over the sheath structure exerted by the lower frequency in combination with the higher current density associated with the higher frequency. Inspection and comparison of eqs. 11 and 18 suggests that the enhancement effect on the Ohmic heating will prove stronger, at least when H_l is large. This is indeed the case. Fig. 6 shows the time-averaged collisionless and Ohmic heating components, with the total heating, as a function of the low-frequency current density, with all other parameters held constant. It is clear that the application of the low-frequency current can produce a transition from a situation that is dominated by collisionless heating to one dominated by Ohmic heating. Of course, whether this

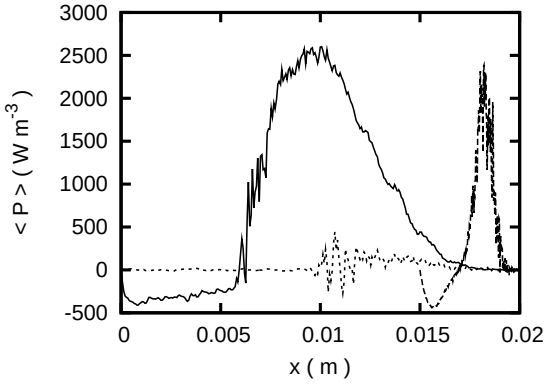

Fig. 4. Time averaged electron heating power resolved in space for three cases corresponding to the two frequencies acting separately and both acting together. Note that the ion sheath edge in each case is approximately located at the transition to negative power absorption, and that the sheath width is appreciably influenced by the application of the high frequency [7], relative to the low frequency acting alone. The parameter values used are $\tilde{J}_l = 10$ A m^{-2}, $\omega_l = 2\pi \times 2$ MHz, $\tilde{J}_h = 36$ A m^{-2} and $\omega_l = 2\pi \times 26$ MHz.

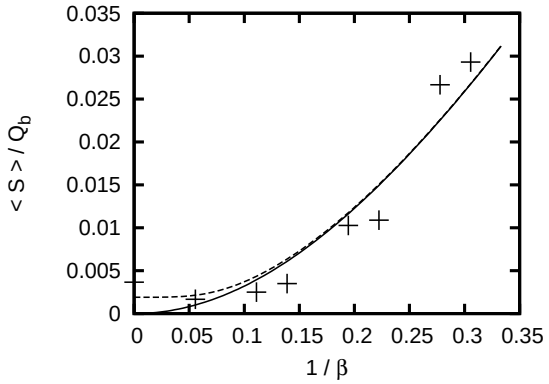

Fig. 5. Time averaged electron heating power as a function of $1/\beta \equiv J_l/J_h$, where the parameter varied is the low frequency current density J_l. Other parameters held constant are the high frequency current density $J_h = 36$ A m^{-2}, and the two frequencies $\omega_l = 2\pi \times 2$ MHz and $\omega_h = 2\pi \times 26$ MHz.

occurs or not also depends on the neutral gas pressure, and in fig. 7 we show the ratio of collisionless to Ohmic heating as a function of low-frequency current density for three disparate gas pressures, covering probably the entire range of practical interest. These data show that it is rather unlikely that a dual frequency discharge used for plasma processing will be dominantly heated by collisionless processes. For example, a typical operating pressure for a dual frequency etching discharge is $\sim$ 50 mTorr, under which condition probably much more than half of the net heating power is Ohmic.

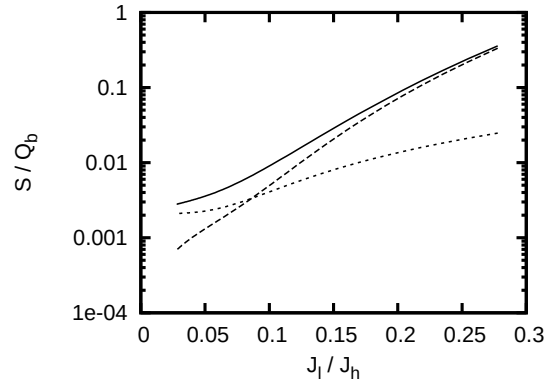

Fig. 6. The collisionless, Ohmic and total heating powers, shown as a function of the low frequency current density. Solid line—total; long dashed line—Ohmic; short dashed line—collisionless.

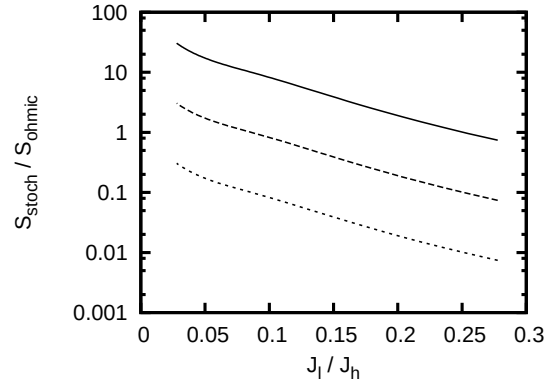

Fig. 7. The ratio of the collisionless and Ohmic heating powers for various electron collision frequencies, corresponding approximately to conditions in argon at pressures of 10 (solid line), 100 (long dashed line) and 1000 mTorr (short dashed line) corresponding to $\nu_e/\omega_l = 3, 30, 300$.

5. Concluding Remarks

In this paper we have developed approximate expressions for collisionless and Ohmic heating of electrons in dual-frequency discharges. These expressions show that both kinds of heating are much affected by the low-frequency current density, because the large voltage associated with that current is the dominant influence on the spatial structure of the sheath region. Although both heating mechanisms are enhanced by the low-frequency current, the effect on Ohmic heating is stronger, with the implication that the dominant heating mechanism can be changed. Indeed, under typical experimental conditions, a discharge that would be dominated by collisionless heating in the absence of a low-frequency

component in the current can become Ohmically dominated when the low-frequency current is applied.

We have neglected a number of issues that may need to be considered in future work. For example, we have assumed that electromagnetic [14] and resonant phenomena [15] may be ignored. We believe this to be reasonable under most experimental conditions today. However, there is a tendency towards increasing the higher frequency in industrial practice, which if continued could vitiate these assumptions. At the moment, nothing is known of the heating mechanisms that might be dominant at very high frequencies. We have also taken rather simple view of the effect of friction on the sheath dynamics. For example, it is known that under some conditions, the sheath electric field may reverse [16], with sometimes dramatic consequences for electron heating. Such effects could occur in dual-frequency discharges.

References

[1] H. C. Kim, J. K. Lee, and J. W. Shon, Phys. Plasmas, 10(11) (2003) 4545–4551.

[2] P. C. Boyle, A. R. Ellingboe, and M. M. Turner, J. Phys. D: Appl. Phys. 37 (2004) 697–701.

[3] F. A. Haas, J. Phys. D: Appl. Phys. 37 (2004) 3117–3120.

[4] J. K. Lee, N.Y. Babaeva, H. C. Kim, O. V. Manuilenko, and J. W. Shon, IEEE Trans. Plasma Sci. 32(1) (2004) 47 – 53.

[5] H. C. Kim and J. K. Lee, Phys. Rev. Lett. 93(8) (2004) 085003.

[6] H. C. Kim and J. K. Lee, Phys. Plasmas 12 (2005) 053501.

[7] J. Robiche, P. C. Boyle, M. M. Turner, and A. R. Ellingboe, J. Phys. D: Appl. Phys. 36 (2003) 1810–1816.

[8] R. N. Franklin, J. Phys. D: Appl. Phys. 36 (2003) 2660–2661.

[9] M. A. Lieberman, IEEE Trans. Plasma Sci. 16(6) (1988) 638–644.

[10] G. Gozadinos, D. Vender, M. M. Turner, and M. A. Lieberman, Plasma Sources Sci. Technol. 10 (2001) 1–8.

[11] M. M. Turner and P. Chabert, Phys. Rev. Lett. 96(20) (2006) 205001.

[12] E. Kawamura, M. A. Lieberman, and A. J. Lichtenberg, Phys. Plasmas 13(5) (2006) 053506.

[13] C. K. Birdsall and A. B. Langdon, Plasma Physics via Computer Simulation, McGraw-Hill, New York, 1985.

[14] P. Chabert, J. L. Raimbault, P. Levif, J. M. Rax, and M. A. Lieberman, Phys. Rev. Lett. 95(20) (2005) 205001.

[15] T Mussenbrock and R-P. Brinkmann, Appl. Phys. Lett. 88(15) (2006) 151503.

[16] M. M. Turner and M. B. Hopkins, Phys. Rev. Lett. 69(24) (1992) 3511–3514.